small NANO MICRO

Templated Synthesis of Shape-Controlled, Ordered TiO_2 Cage Structures

*Yonghui Deng, Harun Tüysüz, Joel Henzie, and Peidong Yang**

Periodically ordered composite materials can be rationally engineered with features spanning nanometer and micrometer length scales.[1–4] As a result, much progress has been made in generating thermally stable metal oxide structures with excellent crystallinity, high surface area, and controllable pore systems for applications in heterogeneous catalysis, fuel cell development, solar energy conversation, photonics, and gas-sensing.[5–10] In this process, the size of the desired features depends on the dimensions of the templates—molecular species including surfactants and block copolymers act as templates for nanoscale pores,[11,12] while colloidal particles template structures with pores in the nano- to microscale size regime.[13–18] Among these templating processes, colloidal crystal templates have gained more attention as new assembly techniques enable larger periodicities. In a typical method, uniformly sized colloidal particles (silica spheres, polymer spheres, or monodisperse nanocrystals) are assembled into 2D or 3D arrays. After formation of the lattice, the space between the particles is filled with a solution containing the precursor of the desired material composition. This precursor is deposited onto the template by drying and annealing the sample. Finally, the original template is selectively etched away to leave a solid crystalline skeleton formed at the interfaces of the colloidal template.[19] Fabrication of monolayer hollow inorganic silica and inorganic hybrid spheres is also reported through the colloid templating route by using electrostatic layer-by-layer self-assembly of silica nanoparticle–polymer multilayers, followed by removal of the polystyrene latex template.[20] Similar solution-templating approaches have generated related cage structures of different material compositions including ZrO_2,[21] CeO_2,[22] TiO_2,[23] SnO_2,[24,25] Cu_2O,[26] Fe_3O_4,[27,28] Co_3O_4,[29] Ag,[30] Au,[31] and Pt.[32]

Dr. H. Tüysüz, Dr. J. Henzie, Prof. P. Yang
Department of Chemistry
University of California
Berkeley, CA 94720, USA
E-mail: p_yang@uclink.berkeley.edu
Dr. H. Tüysüz, Dr. J. Henzie, Prof. P. Yang
Materials Science Division
Lawrence Berkeley National Laboratory
Berkeley, CA 94720, USA
Dr. Y. Deng
Department of Chemistry
Fudan University
Shanghai 200433, P.R. China

DOI: 10.1002/smll.201100579

Alternatively, a more diverse range of material compositions can be accessed using existing gas-phase reaction methods combined with chemical vapor deposition (CVD) or atomic layer deposition (ALD). In a typical CVD or ALD processes, the assembled lattice is exposed to one or more volatile precursors, which then decompose on the substrate surface to produce the desired material.[33] Precise control of the composition and shell thickness of the structure are the biggest advantages of these methods over the solution-templating approach. For example, Zhang et al. used SBA-15 as a hard template and ethylene gas in a CVD approach to prepare ordered mesoporous carbon.[34] And an interesting study was reported by Huang et al. using ALD on the nanostructured surfaces of butterfly wings to template Al_2O_3.[35] ALD synthesis of hollow sphere and nanotube structures composed of Al_2O_3 have been also reported by using spherical nanoparticle and nanorod polymers.[36] Similar approaches have been used to generate pure anatase TiO_2 submicrotubes,[37] by using poly(vinylpyrrolide) fibers as templates, and nanotubes,[38,39] by utilizing anodic alumina templates. In this paper, we report on rational design of unique 2D and 3D cube, cuboctahedra, and octahedra cage structures composed of anatase TiO_2 by assembling Ag nanoparticles into 2D lattices using a Langmuir–Blodgett (LB) technique, or by sedimentation in microfluidic chambers to generate 3D superlattices.

The motivation of this study is the fabrication of high-quality, ordered cage structures of TiO_2 with different shapes and morphologies. The first step on this path is the preparation of an ordered template. LB is a versatile nanoscale bottom-up assembly method that can be used to assemble 2D ordered arrays of Ag polyhedra on a silicon substrate.[40] **Figure 1**a,b shows scanning electron microscopy (SEM) images of close-packed films of cube and octahedra nanoparticles. Figure 1c shows the scheme of the synthetic path of the templating process, where Ag nanoparticles are first coated with amorphous TiO_2 using ALD. After the crystallization of TiO_2, the Ag is selectively removed to create an ordered cage structure. ALD is a powerful approach to deposit high-quality, continuous, ultrathin solid films, where the solid material is formed on a surface using an alternating cycle of self-limiting chemical reactions. This method enables the growth of ultra-uniform thin films with a level of control over film thickness that is difficult to achieve using solution-based methods. The Ag nanoparticle (Ag-NP) arrays were coated with a 20 nm titania shell using titanium tetrachloride as a precursor (200 cycles at 80 °C), and then annealed at 500 °C for 30 min to

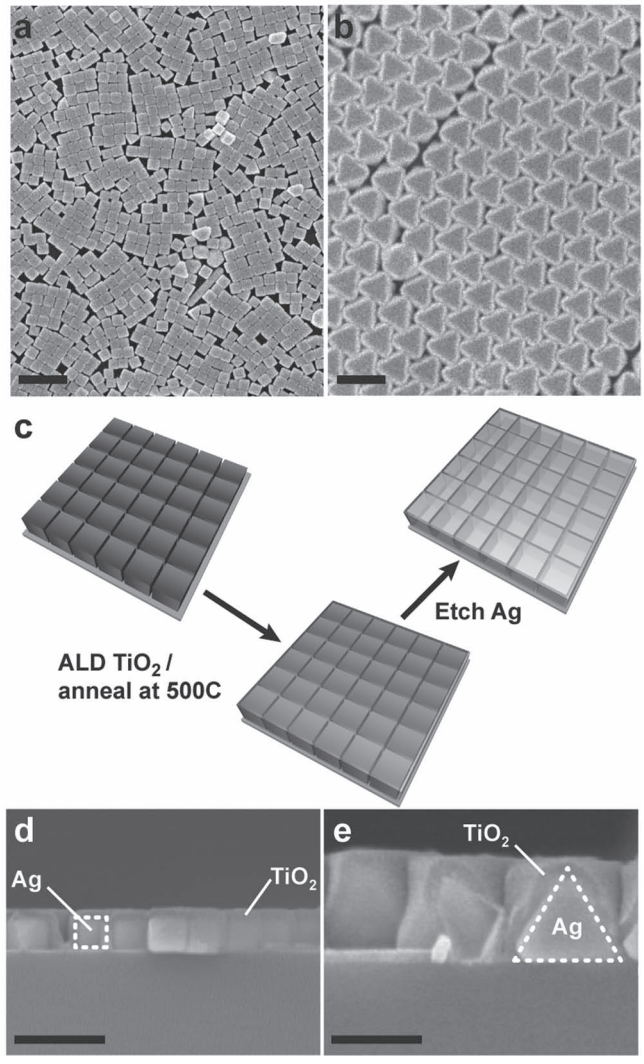

Figure 1. SEM images of close-packed cube and octahedra nanoparticles (a,b) and cross-section core–shell Ag–TiO_2 (d,e), as well as a schematic presentation of the synthetic path of the templating process (c). Scale bars are 300 nm.

crystallize the TiO_2. The morphology of the Ag–TiO_2 composite was investigated by cleaving the sample to expose the cross-section of the Ag-NP–TiO_2 coating (Figure 1d,e). Uniform coating of the TiO_2 shell (20 nm) around the Ag core can be easily observed and the obtained Ag–TiO_2 composite film retains the closely packed 2D array of Ag nanoparticles. In addition, no dramatic change to the shape of the Ag-NP was observed at these temperatures.

After the crystallization of the TiO_2, the Ag template was removed at room temperature by using KI/I_2 aqueous etchant solution. The KI/I_2 solution is a strong oxidizer that can etch away the Ag-NP from the composite by forming AgI. **Figure 2**a–e shows transmission electron microscopy (TEM) micrographs of anatase TiO_2 cage structures formed using cube and octahedral Ag-NPs as templates. SEM images of the cleaved cubic cage structure reveals the 3D view (Figure 2b, insert), showing that the titanium chloride precursor can diffuse into the interstitial spaces between the Ag nanocubes and where it is converted into TiO_2 during the ALD process. Ag-NPs are separated from each other by a polyvinylpyrrolidone (PVP) polymer coating. High-resolution TEM analysis shows crystalline lattice fringes with spacing of 0.35 nm corresponding to {101} planes of anatase titania (Figure 2c). Energy dispersive X-ray analysis (not shown here) confirms that only titanium and oxygen are present in the caged TiO_2 film, and no Ag signal was detected, indicating a complete removal of Ag during the wet etching step. The crystal phase of the cage structure is investigated by X-ray diffraction (XRD). The XRD pattern (Figure 2f) of the caged TiO_2 film shows typical diffraction peaks assigned to pure anatase TiO_2 (Joint Committee on Powder Diffraction Standards No.21-1272).

Ag nanoparticles can be also assembled into complex 3D superlattices by sedimentation in microfluidic chambers.[41] In brief, polyhedra were suspended in a solution of *N*,*N*-dimethylformamide and injected into a 5 cm × 5 cm microfluidic chamber with a thickness of 10 μm. The particles were allowed to sediment and assemble into a large superlattice, and the solvent was removed by evaporation. SEM micrographs show 3D lattices composed of cuboctahedra and octahedra (**Figure 3**a,c). Using the same process as earlier, 3D ordered TiO_2 cages were formed on the surface of the Ag polyhedra, followed by the annealing and etching process. Figure 3b,d show cross-sections of the TiO_2 superlattice cage structures that were sputtered with Au to make them more conductive for SEM imaging. Zoom-in images of the TiO_2 cages show they retain the complex geometry of the superlattices (Figure 3b,d inset). In particular, the inset of Figure 3d shows part of the sputtered nanoscale TiO_2 structure that was templated by the octahedral particle (arrow).

In conclusion, we developed an approach to create high-quality, ordered cage structures of anatase TiO_2 with shape and morphology control by combination of self-assembly and ALD on nanoparticle superlattices. Control of the precise 3D geometry of nanometer to micrometer-scale cage structures has numerous uses in photonic and solar applications such as plasmonics and photocatalysis, where it is important to that the length scale of the structure be on the order of the wavelength of light. This approach can be adapted for the other gas-phase reactions, generating various core-shell and cage structure such as Al_2O_3, SiO_2, ZrO_2, with unique shape and morphology control.

Experimental Section

Chemicals and Materials: Silver nitrate (Aldrich), polyvinylprodine (PVP, M_w 55K Aldrich), 1,5 pentanediol (Across), titanium tetrachloride (Sigma-Aldrich), and absolute ethanol are analytic grade. The gold etchant solution was purchased from Transene Company Inc.

Synthesis of Ag Particles: Silver polyhedral particles (110 nm sized nanocubic particles and 300 nm sized octahedral particles) were prepared according to our previous method.[42] The obtained silver particles were washed with absolute ethanol carefully to remove excess PVP capping agent and dispersed in ethanol for further use.

small NANO MICRO

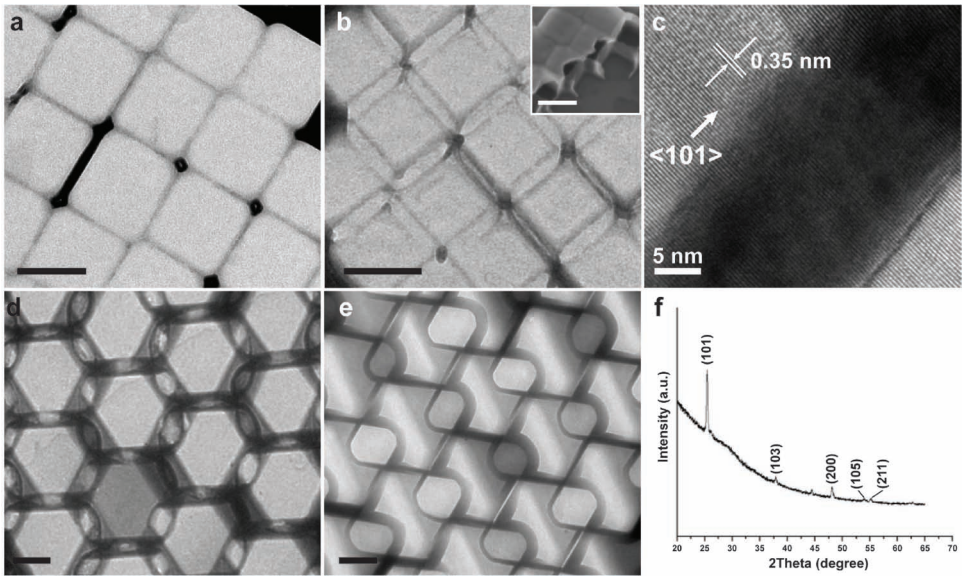

Figure 2. TEM images of cube (a–b) and octahedra (d–e) templated TiO_2 cage structures. Panels (b) and (e) are TEM images of cubic and octahedral cage structures after tilting the sample holder by 15°. The insert in panel (b) is an SEM image of cleaved cubic cage structure. c) High-resolution TEM image of the TiO_2 cage structure; f) XRD pattern of the crystalline anatase phase of the TiO_2 cage structure. All unmarked scale bars are 100 nm.

Fabrication of Ag NP–TiO_2 Composite Film and the Derived Caged TiO_2 Film: Freshly cleaned small Si substrate (0.9 cm × 0.9 cm) is first coated with a 20 nm-thick amorphous titania by atomic layer deposition (ALD) at 80 °C using tetrachloride titanium as the precursor, and Ag nanoparticles (cube and octahedra) are then deposited on the substrate surface by using Langmuir–Blodgett (LB) technique (NIMA type 611). After drying in nitrogen atmosphere, the Ag LB films were coated with another layer of amorphous titania using ALD method at 80 °C to achieve a complete encapsulation of Ag nanoparticles. Finally, the obtained composite films on quartz substrates were annealed at 500 °C for 30 min in argon atmosphere, resulting in crystallized Ag–TiO_2 composite films. 20 nm thickness of the titania is an optimized condition in this study. After the crystallization step, Ag nanoparticles are selectively etched with KI/I_2 aqueous solution. Typically, a piece of Si plate with Ag–TiO_2 composite film was soaked in 5 mL of etchant solution overnight, and afterwards, the etched sample was thoroughly washed with deionized water and ethanol sequentially, and finally dried by carefully blowing nitrogen gas.

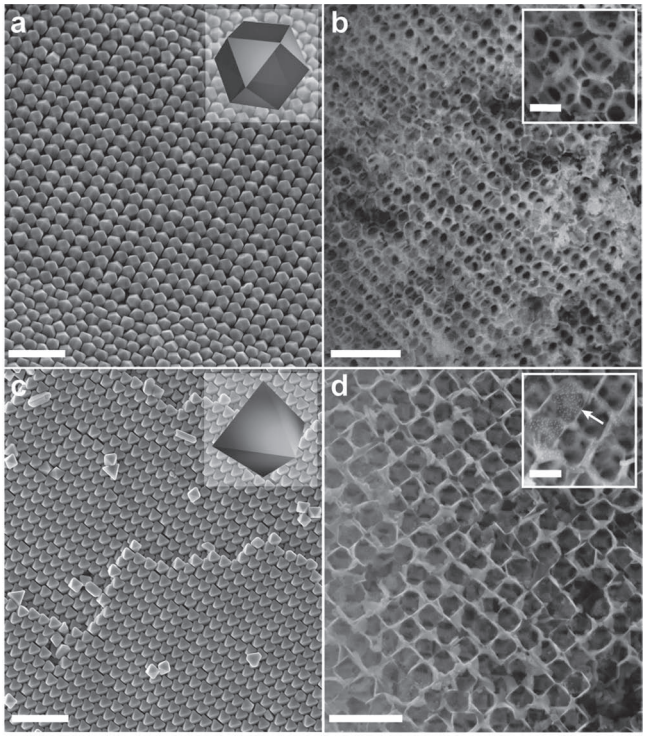

Figure 3. SEM images of 3D lattice of cuboctehedra (a) and octahedra (c) Ag nanoparticle and 3D cage structure of cuboctehedral (b) and octahedral (d) TiO_2 replica. The scale bars are 1 μm for images and 250 nm for the insets.

Self-Assembly of 3D Superlattices in Microfluidic Chambers: Polydimethylsiloxane (PDMS) chambers were designed to template 3D lattices with millimeter-scale lateral dimensions that are ≈20 μm in height. Four 100 μm wide, ≈1 mm long inlets were included at the top of the chamber to reduce PDMS sagging inside the chamber and minimize any effects of solvent evaporation during assembly experiments. Negative tone photoresist (SU-8 25; Microchem) was spin-cast on Si wafers (3000 r.p.m., 40 s), baked (95 °C, 3 min), exposed to UV light using a high-resolution transparency photomask, then post-baked and developed to produce master patterns. PDMS prepolymer (Sylgard-184) was poured on the masters and cured thermally (70 °C, 24 h). Then the PDMS chamber was removed from the master and placed on Si or glass that had been passivated with tridecafluoro-1,1,2,2-tetrahydrooctyl-1-trichlorosilane (Gelest, Inc.). All assembly experiments were performed under a crystallization dish to further reduce solvent evaporation. The PDMS chamber setup was tilted 15° from horizontal and filled with dimethyformamide (DMF). 2 μL of DMF solution containing Ag polyhedra (0.351 mg μL^{-1} (w/v) for octahedra) was loaded on the top of the device and allowed to sediment into the chamber through the inlets. Progress during

assembly was monitored using dark-field scattering microscopy. Prior to SEM imaging, the assembly setup was dried in air for several hours, and the PDMS chamber could be removed.

Characterization: Scanning electron microscope images were obtained using a field emission scanning electron microscope (FESEM, JEOL6430) operated at an accelerating voltage of 5 kV. Wide angle X-ray diffraction measurement was carried out on Bruker D8 X-ray diffractometer. Transmission electron microscopy images were taken on Hitachi H-7650 (120 kV). High-resolution TEM images were taken on a transmission electron microscope Philips CM200/FEG, operated at 200 kV. Absorption spectrum was taken by using integrating sphere (Shimatzu). UV–vis–NIR spectra were measured using a Shimadzu UV-3101 PC spectrophotometer.

Acknowledgements

This work is supported by AFOSR. Y.D. thanks the China Scholarship Council (CSC) for sponsoring oversea visiting research. H.T. thanks the German Research Foundation (DFG) for the research fellowship.

This Communication is part of the Special Issue dedicated to Chad Mirkin in celebration of 20 years of influential research at Northwestern University.

[1] A. H. Lu, F. Schüth, *Adv. Mater.* **2006**, *18*, 1793.
[2] M. Tiemann, *Chem. Mater.* **2008**, *20*, 961.
[3] B. Tian, X. Liu, H. Yang, S. Xie, C. Yu, B. Tu, D. Zhao, *Adv. Mater.* **2003**, *15*, 1370.
[4] O. D. Vele, E. W. Kaler, *Adv. Mater.* **2000**, *12*, 531.
[5] H. Tüysüz, M. Comotti, F. Schüth, *Chem. Commun.* **2008**, 4022.
[6] R. C. Schroden, M. Al-Daous, C. F. Blanford, A. Stein, *Chem. Mater.* **2002**, *14*, 3305.
[7] G. S. Chai, L. S. Shin, J. S. Yu, *Adv. Mater.* **2004**, *16*, 2057.
[8] T. Brezesinski, D. F. Rohlfing, S. Sallard, M. Antonietti, B. M. Smarsly, *Small* **2006**, *2*, 1203.
[9] M. D. Wei, Y. Konishi, H. S. Zhou, M. Yanagida, H Sugihara, H. Arakawa, *J. Mater. Chem.* **2006**, *16*, 1287.
[10] T. Waitz, T. Wagner, T. Sauerwald, C. D. Kohl, M. Tiemann, *Adv. Funct. Mater.* **2009**, *19*, 653.
[11] C. T. Kresge, M. E. Leonowicz, W. J. Roth, J. C. Vartuli, J. S. Beck, *Nature* **1992**, *359*, 710.
[12] P. Yang, D. Zhao, D. I. Margolese, B. F. Chmelka, G. D Stucky, *Nature* **1998**, *396*, 152.
[13] G. Subramanian, V. N. Manoharan, J. D. Thorne, D. J. Pine, *Adv. Mater.* **1999**, *11*, 1261.
[14] P. N. Bartlett, J. J. Baumberg, P. R. Birkin, M. A. Ghanem, M. C. Nett, *Chem. Mater.* **2002**, *14*, 2199.
[15] B. T. Holland, C. F. Blanford, T. Do, A. Stein, *Chem. Mater.* **1999**, *11*, 795.
[16] F. Li, Y. Qian, A. Stein, *Chem. Mater.* **2010**, *22*, 3226.
[17] K. D. Hartlen, A. P. T. Athanasopoulos, V. Kitaev, *Langmuir* **2008**, *24*, 1714.
[18] Y. Kuroda, K. Kuroda, *Angew. Chem. Int. Ed.* **2010**, *49*, 6993.
[19] A. Stein, *Microporous Mesoporous Mater.* **2001**, *44-45*, 227
[20] F. Caruso, R. A. Caruso, H. Mohwald, *Science* **1998**, *282*,1111.
[21] P. M. Arnal, C. Weidenthaler, F Schüth, *Chem. Mater.* **2006**, *18*, 2733
[22] N. C. Strandwitz, G. D. Stucky, *Chem. Mater.* **2009**, *21*, 4577.
[23] F. Caruso, X. Y. Shi, R. A. Caruso, A. Susha, *Adv. Mater.* **2001**, *13*, 740.
[24] C. J. Martinez, B. Hockey, C. B. Montgomery, S. Semancik, *Langmuir* **2005**, *21*, 7937.
[25] H. P. Cong, S. H. Yu, *Adv. Funct. Mater.* **2007**, *17*, 1814.
[26] X. W. Lou, C. Yuan, L. A. Archer, *Small* **2007**, *3*, 261.
[27] F. Caruso, M. Spasova, A. Susha, M. Giersig, R. A. Caruso, *Chem. Mater.* **2001**, *13*, 109.
[28] M. Yang, J. Ma, C. L. Zhang, Z. Z. Yang, Y. F. Lu, *Angew. Chem. Int. Ed.* **2005**, *44*, 6727
[29] T. He, D. R. Chen, X. L. Jiao, Y. L. Wang, *Adv. Mater.* **2006**, *18*, 1078.
[30] D. B. Zhang, L. M. Qi, J.M. Ma, H. M. Cheng, *Adv. Mater.* **2002**, *14*, 1499.
[31] Z. J. Liang, A. Susha, F. Caruso, *Chem. Mater.* **2003**, *15*, 3176.
[32] X. W. Lou, C. Yuan, Q. Zhang, L. A. Archer, *Angew. Chem. Int. Ed.* **2006**, *45*, 3825
[33] M. Leskela, M. Ritala, *Thin Solid Films* **2002**, *409*, 138.
[34] W. H. Zhang, C. Liang, H. Sun, Z. Shen, Y. Guan, P. Ying, C. Li, *Adv. Mater.* **2002**, *14*, 1776.
[35] J. Huang, X. Wang, Z. L. Wang, *Nano Lett.* **2006**, *6*, 2325.
[36] R. H. A. Ras, M. Kemell, J. de Wit, M. Ritala, G. ten Brinke, M. Leskelä, O. Ikkala, *Adv. Mater.* **2007**, *19*, 102.
[37] G. M. Kim, S. M. Lee, G. H. Michler, H. Roggendorf, U. Gosele, M. Knez, *Chem. Mater.* **2008**, *20*, 3087.
[38] L. K. Tan, M. A. S. Chong, H. Gao, *J. Phys. Chem. C* **2008**, *112*, 69
[39] M. S. Sander, M. J. Cote, W. Gu, B. M. Kile, C. P. Tripp, *Adv. Mater.* **2004**, *16*, 2052.
[40] A. Tao, S. Habas, P. Yang, *Small* **2008**, *4*, 310.
[41] J. Henzie, M. Gruenwald, A. Widmer-Cooper, P. Geissler, P. Yang, **2011**, unpublished.
[42] A. Tao, P. Sinsermsuksakul, P. Yang, *Angew. Chem. Int. Ed.* **2006**, *45*, 4597.

Received: March 24, 2011
Published online: June 14, 2011